Séminaire Poincaré IX (2006) 91 – 114 **Séminaire Poincaré**

Instruments for Gravitational Wave Astronomy on Ground and in Space

Jean-Yves Vinet
ARTEMIS
Observatoire de la Côte d'Azur
Nice – France

Abstract. Gravitational Wave Astronomy progressively becomes this new window on the universe that we expected since tens of years. The technology has now reached a point where large instruments meet a level of sensitivity relevant for astrophysics. Depending on the sector of physics to be addressed, i.e. depending on the frequency domain, ground or space instruments are required. Ground based antennas are already built in Europe, in Japan and in the USA and begin to deliver science data. The ESA/NASA space mission LISA is not yet definitively approved, but a number of teams endeavour to successfully pass the coming project reviews. We review the general principles of the optical detection of gravitational waves.

1 Introduction

More and more highly relativistic objects are directly seen even in our galaxy. These objects are mainly compact systems involving neutron stars or black holes ending by an inspiral phase of variable time duration. Systems involving objects of stellar class (up to a few tens of solar masses) on compact orbits emit gravitational waves (GW) roughly in the acoustic band (from a few Hz to a few kHz), whereas more heavy systems, and especially supermassive black holes are expected to cause gravitational events of very low frequency (below 0.1 Hz). General Relativity simultaneously provides models for these processes where strong gravity deeply differ from Newtonian theory, and the right messenger (GW) for carrying the relevant information. For uncoding this information, several types of GW antennas have been proposed in the past, and a few of them survive under the form of large instruments or projects on Earth or in space. The fact that the expected dimensionless amplitudes of GW correspond to a space-time strain amplitude less than 10^{-22} is the cause of all technological issues encountered during the R&D phase of all projects. At this level, all possible environmental or instrumental noise sources must be carefully investigated, and solutions must be found in order to obtain a signal to noise ratio consistent with the observational goals. For ground based instruments like LIGO [1] and Virgo [2], the most challenging issues were the seismic insulation, the vacuum system, the mirrors processing, the laser stabilization. The ultimate residual fundamental noises are the shot noise and the thermal noise. For a space mission like LISA [3], the main issues were the long optical links, the drag-free operation and the rejection of the lasers frequency noise. This paper aims to point and briefly discuss the physics underlying some of the technical challenges of this extreme metrology.

2 Gravitational Waves

2.1 GW emission

Gravitational waves (GW) are a consequence of Einstein's General Relativity (GR) as electromagnetic waves come from Maxwell's Electrodynamics. In the framework of Special Relativity, in a system of coordinates x^λ, an electromagnetic wave is described

(in vacuum) by the vector field $A_\mu(x^\lambda)$ (4-potential) obeying the Maxwell equations. The wave propagates at velocity c, is transverse and has two polarization components. In GR, the gravitational state of spacetime is associated to its geometry through the metric tensor $g_{\mu\nu}(x^\lambda)$ obeying the Einstein equations. In the case of a gravitational wave far from its source, in a freely falling reference system, one can write:

$$g_{\mu\nu}(t,\mathbf{x}) \;=\; \eta_{\mu\nu} + h_{\mu\nu}(t,\mathbf{x}) \tag{1}$$

where $\eta_{\mu\nu} \equiv \mathrm{diag}(1,-1,-1,-1)$ is the Minkowski tensor of the locally flat background spacetime (freely falling frame), and $h_{\mu\nu}$ a very small dimensionless tensor field representing the GW amplitude. It can be shown that $h_{\mu\nu}$ can be eventually reduced to only two independent functions $h_+, h_\times$ defining the polarization state of the wave. Gravitational waves are emitted by distributions of matter/energy having a time dependent quadrupole moment. In the transverse-traceless gauge, at the first level of approximation, only the space components are significant and have an expression analogous to a retarded potential [4]:

$$h_{jk}(t,r) \;=\; \frac{2G}{c^4}\frac{1}{r}\,\partial_t^2\,\left[\Xi_{jk}(t-r/c)\right]^{\mathrm{TT}} \tag{2}$$

($r \equiv \mathbf{x}^2$) where the symbol TT refers to the projection on the transverse plane of the symmetric traceless quadrupole tensor $\Xi(t)$ defined by the volume integral:

$$\Xi_{jk}(t) \;=\; \int \rho(t,\mathbf{x})\left[x^i x^j - \frac{1}{3}\,\delta_{jk}\,\mathbf{x}^2\right] d^3x$$

where ρ is the density of matter. Further levels of approximation have been deeply investigated [5], but the preceding "quadrupole formula" gives an order of magnitude. One immediately notes the extreme weakness of the coupling coefficient G/c^4 which is the cause of all technological challenges encountered on the way to GW astronomy. Only astrophysical events involving stars or black holes in nearly relativistic velocity regime can cause amplitudes of GW larger than 10^{-25} in the neighborhood of the Earth. The most promising candidates are the final inspiralling of compact binaries. The frequency domain of the waves is determined by the masses of the components of the binary. Stellar class binaries can end at 1 kHz whereas Massive Black Holes can end at a small fraction of a Hz. The observation instruments must change according to the addressed domain of frequency. Existing instruments have been designed for a sensitivity of about 10^{-23} at the middle of the bandwidth, which seemed the best feasible at the time when the preliminar R&D studies ended.

2.2 Physical signature of a GW

Being a perturbation of the geometry of spacetime, one can expect GW to produce distortions in some metrology experiments. We briefly recall the existence of narrow band solid antennas, then focus on optical experiments.

2.2.1 GW and continuous media

The first experiment proposed by Weber [6] rested on the idea that a GW could induce stresses in solids, and that on a suitably isolated solid resonator, weakly dissipative for acoustic waves, one could detect with some transducer system the resonances occurring when the GW signal overlaps its acoustical bandwidth. This idea is supported by a general relativistic extension of the linear elasticity theory [7]. A result is the modified tensor elastodynamic equation:

$$\rho\ddot{E}_{ij} - \frac{1}{2}\left[\partial_k\partial_j\Theta_{ik} + \partial_k\partial_i\Theta_{jk}\right] \;=\; -\frac{1}{2}\,\rho\,\ddot{h}_{ij} \tag{3}$$

Where E_{ij} (resp. Θ_{ij}) is the classical strain (rep. stress) tensor, and ρ the density. If we take the origin of coordinates at the center of mass, and if we assume a GW wavelength much larger than the size of the resonator, this can be regarded as a derivative of the following vector elastodynamic equation:

$$\rho \ddot{u}^i - \partial_k \, \Theta^{ik} \;=\; -\frac{1}{2}\,\rho\, \ddot{h}^{ij} x^j \tag{4}$$

where $\mathbf{u}$ is the displacement vector. The GW amplitude appears thus as a driving internal (of tidal type) force acting on the resonator. After the controversial but negative results of Weber, several groups nevertheless built hugely improved versions of the Weber antenna. These instruments called "bar antennas" have been built in several countries [8],[9], and even larger resonators having spherical shapes are planned [10]. As any resonator, bars have a very short bandwidth (up to a few tens of Hz), so that reconstructing a waveform after a detected GW event is problematic. This is why we focus on optical experiments which are intrinsically wideband.

2.2.2 GW and light

A more direct physical effect of GW is to modulate the light distances between freely falling test masses. In vacuum, light is expected to propagate along a null geodesic, which means that the invariant element of spacetime $ds^2 \equiv g_{\mu\nu} dx^\mu dx^\nu$ is identically zero along any optical path. with the expression (1) of the metric tensor, one can suspect that the effective optical paths of photons will be perturbed.

Detectors of size much smaller than the GW wavelength The expected frequencies of GW events for obvious reasons are much lower (at most a few kHz) than optical frequencies. In this regime, the only effect of a GW on light is to perturb the flight time of photons between two test masses (light distances). Consider a light path lying in the (x, y) plane, either along the x (north) or the y (west) axis. Consider on the other hand a GW propagating along a direction of unit vector $\mathbf{w}$.

$$\mathbf{w} \;=\; \begin{pmatrix} \sin\theta\cos\phi \\ \sin\theta\sin\phi \\ \cos\theta \end{pmatrix} \tag{5}$$

If $h_+, h_\times$ are the two polarization components of the wave, the effect of the GW is to create a phase modulation on the two beams:

$$\Phi_{\rm north}(t) \;=\; \frac{2\pi L}{\lambda}\,\left[h_+(t)(\cos^2\theta\cos^2\phi - \sin^2\phi) - h_\times(t)\cos\theta\sin 2\phi\right] \tag{6}$$

$$\Phi_{\rm west}(t) \;=\; \frac{2\pi L}{\lambda}\,\left[h_+(t)(\cos^2\theta\sin^2\phi - \cos^2\phi) + h_\times(t)\cos\theta\sin 2\phi\right] \tag{7}$$

In an interferometric configuration, where the observable is a differential phase, this gives:

$$\Delta\Phi(t) \;=\; \frac{4\pi L}{\lambda}\,\left[h_+(t)\,\frac{1+\cos^2\theta}{2}\,\cos 2\phi - h_\times(t)\cos\theta\sin 2\phi\right] \tag{8}$$

where it can be seen that the interferometer acts like a transducer, converting the gravitational signal into a phase and eventually into an electrical signal through some photo detector.

Detectors of size comparable to the GW wavelength In the case of very long range optical paths (e.g. 5 Mkm in the case of LISA), one must take into account the action of the GW during light propagation. If a light beam of fixed frequency is emitted from spacecraft A and detected at spacecraft B, the nominal distance AB being L

and $\mathbf{n}$ the unit vector from A to B, the physical effect detected at B is a frequency modulation. Let $\mathbf{w}$ be again the propagation unit vector of the GW, and let us define two more unit vectors mutually orthogonal in the transverse plane:

$$\vartheta \;=\; \frac{\partial \mathbf{w}}{\partial \theta}, \quad \varphi \;=\; \frac{1}{\sin\theta}\,\frac{\partial \mathbf{w}}{\partial \phi}$$

then the two directional functions

$$\xi_+(\theta,\phi) \;=\; (\vartheta.\mathbf{n})^2 - (\varphi.\mathbf{n})^2, \quad \xi_\times(\theta,\phi) \;=\; 2(\vartheta.\mathbf{n})(\varphi.\mathbf{n})$$

then the function

$$H(t) \;=\; h_+(t)\,\xi_+(\theta,\phi) \;+\; h_\times\,\xi_\times(\theta,\phi). \tag{9}$$

Now the observable is a relative frequency modulation, analogous to a Doppler shift [11] given by:

$$\left[\frac{\delta\nu(t)}{\nu}\right]_{A\to B} \;=\; \frac{H(t-\mathbf{w}.\mathbf{x}_B) - H(t-\mathbf{w}.\mathbf{x}_A - L)}{2(1-\mathbf{w}.\mathbf{n})} \tag{10}$$

where $\mathbf{x}_A$ and $\mathbf{x}_B$ are the positions of the two spacecraft . This is often called a "two pulses" response because a short GW pulse would have this double effect on a phasemeter at B.

3 Ground based detectors

3.1 General principles

3.1.1 Interferometers

A Michelson interferometer involves a splitter sharing a laser light into two secondary beams that recombine on it after a reflection on far mirrors, generating interferences on a photodetector. Such a device generates a phase quantum (shot) noise due to the quantum nature of light detection and characterized by the white power spectral density (PSD)

$$S(f) \;=\; \frac{2\hbar\omega}{P_L}$$

where $\lambda \equiv 2\pi c/\omega$ is the laser wavelength and P_L its power. The quantum efficiency of the photodetector has been taken equal to 1. If according to (8), the differential phase induced by the GW is at most (single and optimal polarization, normal incidence):

$$\Delta\Phi(t) \;=\; \frac{4\pi L}{\lambda}\,h(t)$$

the result is that the ultimate, shot-noise limited sensitivity of a simple Michelson having two orthogonal arms of length L is given by the white linear spectral density (LSD):

$$S_h^{1/2} \;=\; \frac{\lambda}{4\pi L}\sqrt{\frac{2\hbar\omega}{P_L}} \tag{11}$$

It is easily seen that even with large parameters ($L = 3$ km, $P_L = 20$ W), the result ($\sim 4\,10^{-21}$ $\mathrm{Hz}^{-1/2}$) is far from the requirements. It is seen as well that increasing these already big parameters is not so easy. Solutions have been proposed years ago by R. Drever [12].

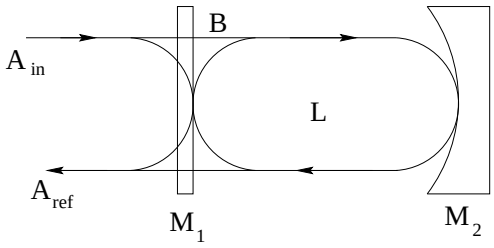

Figure 1: Fabry-Perot cavity

3.1.2 Resonant Fabry-Perot cavities

The leading idea is to use the properties of resonant cavities firstly for increasing the effective lengths of the arms, and secondly for increasing the effective power reaching the splitter. Consider a resonant (Fabry-Perot) cavity of length L, having an input mirror of reflectivity r_1, an end mirror of reflectivity r_2 (see Fig.1). If a wave of amplitude $A_{\rm in}$ arrives at the input M_1 mirror, it is partially transmitted by M_1 and partially reflected, the transmitted part propagates to M_2, is reflected, propagates back to M_1 where it is partially transmitted and partially reflected. The mirrors have some weak relative losses p so that their transmission t and reflection r coefficients are related by the relative power balance $r^2 + t^2 = 1 - p$. Moreover, there must be a $\pi/2$ phase lag between the reflected part and the transmitted part, so that t and r being real numbers, we use ir as the reflection and t as the transmission operator. operator. One can write therefore the steady state equation, assuming B as the intracativy amplitude :

$$B \;=\; t_1\, A_{\rm in} - r_1 r_2 {\rm e}^{2ikL}\, B \tag{12}$$

where λ is the wavelength and $k \equiv 2\pi/\lambda$. On the other hand, the reflected amplitude is the sum of the directly reflected wave and the one partially transmitted from inside the cavity :

$$A_{\rm ref} \;=\; ir_1 A_{\rm in} + ir_2 t_1 B$$

all this put together gives the global reflectance of the cavity :

$$\mathcal{R} \;=\; A_{\rm ref}/iA_{\rm in} \;=\; \frac{r_1 + (1-p_1) r_2 {\rm e}^{2ikL}}{1 + r_1 r_2 {\rm e}^{2ikL}}$$

Eq.(12) has the obvious solution

$$B \;=\; \frac{t_1}{1 + r_1 r_2 {\rm e}^{2ikL}}\, A_{\rm in}$$

which makes clear that a resonance occurs, giving a peak of stored power when the round trip phase $2kL$ is an odd multiple of π. Instead of r_1, r_2, L, a new set of relevant parameters are:

- The finesse $\mathcal{F}$ given by

$$\mathcal{F} \;=\; \frac{\pi\sqrt{r_1 r_2}}{1 - r_1 r_2} \tag{13}$$

- The free spectral range $\Delta\nu$ or frequency gap between two successive resonances:

$$\Delta\nu \;=\; \frac{c}{2L} \tag{14}$$

- The linewidth $\delta\nu$ defined by:

$$\delta\nu \;=\; \Delta\nu/\mathcal{F} \tag{15}$$

One can show that in such a cavity tuned at resonance:

- The reflectance of the cavity as a whole is:

$$\mathcal{R}_0 \;=\; 1-\sigma$$

where the coupling coefficient σ is

$$\sigma \;=\; p\mathcal{F}/\pi \tag{16}$$

$p \equiv p_1+p_2$ being the total relative light power loss of the cavity (thermalization, diffraction...).

- The phase change of the reflected wave on a very tiny displacement δL of the end mirror is

$$\delta\Phi \;=\; \frac{8\mathcal{F}}{\lambda}\,\delta L$$

If we compare to the phase change due to the same displacement without input mirror (with only the end mirror)

$$\delta\Phi \;=\; \frac{4\pi}{\lambda}\,\delta L,$$

we see that the cavity has an effect equivalent to $\mathcal{S} = 2\mathcal{F}/\pi$ round trips. For a finesse of 50, as currently planned, the result is equivalent, in terms of h to an arm of length $L_{\rm eff} \sim 100$ km.

- If we compute the power $P_{\rm stored}$ stored at resonance we obtain as long as $\sigma \ll 1$:

$$P_{\rm stored} \;=\; \frac{2\mathcal{F}}{\pi}\,P_{\rm inc}$$

where $P_{\rm inc}$ is the power reaching the input mirror. Parameter $\mathcal{S} = 2\mathcal{F}/\pi$ is called surtension coefficient. It is equal to the effective number of round trips in the cavity.

3.1.3 Recycling interferometers

These interesting properties of resonant cavities are the basis of all optical GW antennas. On Fig.2, one can see the principles of Virgo (for instance). It can be shown that the optimal sensitivity of a shot noise limited interferometer is reached when the extinction of the outgoing beam (to photodetector) is a maximum. The whole Michelson section (the two arms plus the splitter) act therefore as a virtual mirror, and adding one more mirror (the recycler) builds a new cavity, called the recycling cavity: one may imagine that the light almost totally reflected by the Michelson re-enters the interferometer. In other words, the recycler carries out an impedance matching between the laser and the Michelson. Starting from a 20 W laser, a first resonance increases to 1 kW the power reaching the splitter. After splitting, 500 W are fed into the long cavities, and the power stored in these is about 15 kW. The finesse of the arm cavities was fixed at $\mathcal{F}$ =50, increasing the effective length of the arms by a factor of about 30 giving 90 effective km, and the surtension coefficient of the recycling cavity at $\mathcal{S} = 50$. The total gain factor with respect to a simple Michelson is better than 200 according to (11), giving a LSD of h equivalent to shot noise of about $2\,10^{-23}\,\mathrm{Hz}^{-1/2}$, consistent with the requirements. This spectral density is not white any more however, because the transfer function from GW to detected phase falls to zero when the GW frequency is larger than the linewidth of the long cavities (or when the GW wavelength becomes shorter than the effective lengths of the arms as well). The complete LSD of h equivalent to shot noise is:

$$S_h^{1/2}(f) \;=\; \frac{\lambda}{8\mathcal{F}L}\sqrt{\frac{2\hbar\omega}{P_L}}\,\frac{1}{\sqrt{\mathcal{S}}}\,\sqrt{1+4(f/\delta\nu)}^2 \tag{17}$$

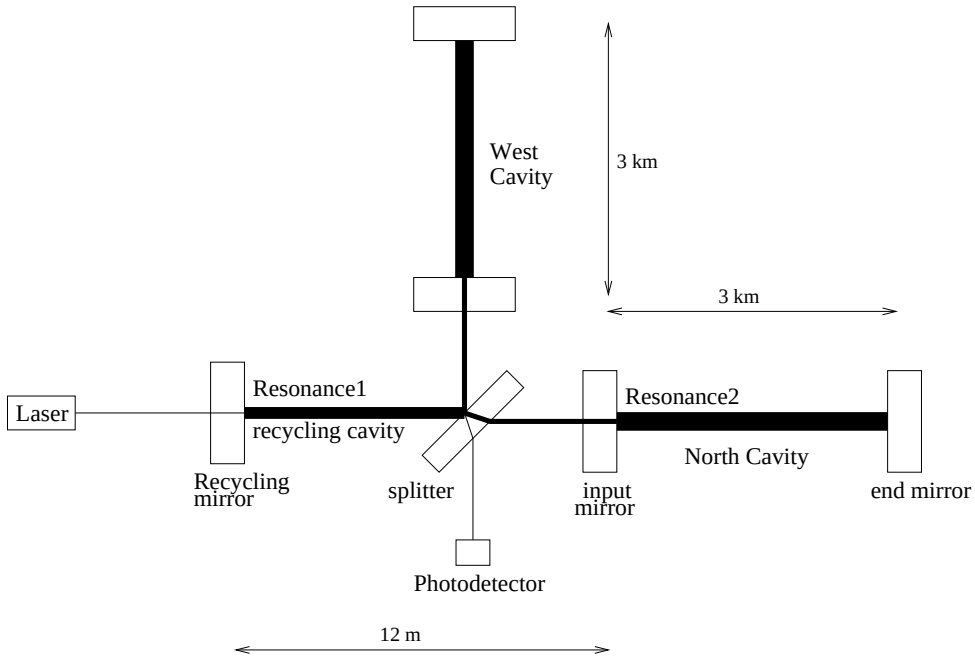

Figure 2: Sketch of a recycling Fabry-Perot interferometer

where one sees the effect of $\mathcal{F}$ for increasing the arm length, and of $\mathcal{S}$ for increasing the laser power. Shot noise is not however the only fundamental limit to that kind of metrology.

3.2 The insulation challenge

There is no way to distinguish GW action on the space between mirrors and spurious motion of these. At the level of about 10^{-20}m.Hz$^{-1/2}$, the causes of spurious motion are a number. In particular, there is no hope to reach the fundamental limits without a very efficient insulation system.

3.2.1 Seismic insulation

The mirrors are suspended by thin wires in order to be almost free in the horizontal plane for small motions (approximation of a free fall). All optical antennas have therefore a more or less sophisticated filtering system. The complexity of the filter depends on the fixed "wall" frequency i.e. the lower frequency bound. For a wall at 50 Hz, classical acoustic filters as the LIGO's work. For pushing back the wall to 10 Hz, a more complex system was devised for Virgo. It is well known that the oscillations y of a pendulum are related to those x of its suspension point by a transfer function (TF) of the form

$$\frac{\tilde{y}(f)}{\tilde{x}(f)} = \frac{1}{1 - f^2/f_0^2}$$

where f_0 is the resonance frequency. There is thus an attenuation factor of f_0^2/f^2 for frequencies much larger than the resonance. The idea of a so-called "superattenuator" was to construct a chain of n pendulums able to oscillate with very low resonance frequencies along all degrees of freedom (vertical and horizontal). The global TF is approximately the product of all elementary TFs, or $(f_0/f)^{2n}$ assuming comparable resonance frequencies. The pendulums are essentially heavy masses ($\sim$ 100 kg)

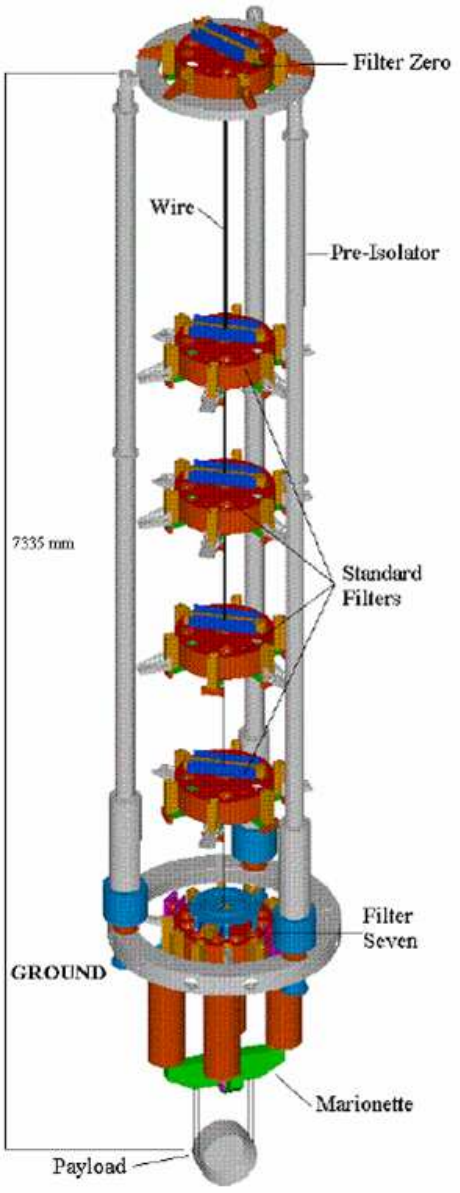

Figure 3: Superattenuator developed at Pisa

suspended by 1m long wires giving a resonance at about 0.5 Hz for the horizontal motion, and containing steel blades whose bending stiffness has been reduced by magnets (negative spring) for the vertical motion. A global attenuation factor of about 10^{-14} at 10 Hz is obtained this way. See on Fig.3 the details of a superattenuator.

3.2.2 Vacuum

Suppressing the refraction index fluctuations due to air pressure fluctuations requires operating in an ultravacuum. The residual hydrogen pressure must be lower than 10^{-9} mbar and 10^{-14} mbar for hydrocarbons. All the optical system and the suspensions must therefore be installed in a high quality vacuum system. The steel pipelines containing the cavities have 1.2 m diameter and 3 km long. This represents an area of more than 20,000 m^2. An important and successful item in the R&D program was

Figure 4: Global view of Virgo at Cascina (Italy)

to find the thermal treatment of stainless steel able to suppress the outgassing rate at the required level in order to avoid operating with a continuous pumping. The external aspect of ground based detectors is determined by this huge vacuum system (see the example of Virgo on Fig.4).

3.3 Fighting the thermal noise

The second fundamental limit in the sensitivity comes from the fact that the optical system essentially reads the distance between the reflecting surfaces of two mirrors (in each cavity). It is thus clear that any spurious motion of these surfaces competes with the gravitational signal. Once eliminated unessential causes of motion (sound waves, seismic vibrations...) by the insulation system, it remains sources of motion in the thermal random excitation inside all material elements of the system holding the mirrors. As seen above, the filtering chain suspending the mirrors is a series of harmonic oscillators coupled with the mirror's motions. The mirrors themselves, that are thick (10 cm) and wide (35 cm diameter) silica cylinders may be considered as solid resonators and have elastodynamic modes disturbing their shapes and resulting in an apparent displacement. The resulting noise in the readout system is called thermal noise. Three different sectors of thermal noise can be distinguished:

- The thermal excitation of the pendulum chain suspending the mirror holder. The corresponding spectral density fixes the wall frequency at 10 Hz
- The thermal excitation of the wires holding the mirrors from the last pendulum stage. The resonances of these wires are called "violin modes". These resonances can be sharpened by using high Q materials and weldings. The present trend is to use monolithic silica suspensions.
- The internal modes of the mirrors substrates give a PSD of noise with a low frequency tail dominating all noises in the 100 Hz region.

The region of 100 Hz being very intersting from the astrophysics point of view, a number of efforts have been spent for finding ways of reducing the mirrors thermal noise. This is why we put a special emphasis on this particular sector of past and current R&D efforts. Let us discuss the proposed ideas.

3.3.1 Cooling

The PSD of thermal noise is proportional to the temperature T, so that cooling is an obvious good idea. But the LSD is proportional to $\sqrt{T}$ so that in order to gain 1 order of magnitude in sensitivity, one must reach cryogenic temperatures. Some R&D has been carried out by a Japanese team [13] in the LCGT project.

3.3.2 New materials

The PSD of thermal noise of any oscillator depends also on its mechanical quality factor. The quality factor of a compound system is determined by the intrinsic mechanical dissipation rate in the used materials but also by the way they are assembled. In the present situation, for instance in Virgo, the mirrors are suspended by thin steel wires. More specifically it has been shown [14] that so far as the internal thermal the low frequency tail of the PSD of displacement equivalent to thermal noise is:

$$S_x(f) \;=\; \frac{4k_BT}{\pi f}\,\phi\,U \tag{18}$$

where k_B is the Boltzmann constant, ϕ a loss angle (inverse of a quality factor) and U the strain energy stored in the solid substrate under a pressure distribution having the profile of the readout optical beam and normalized to 1 N resulting force. The second parameter to play with is the loss angle ϕ. It seems that it is difficult to have loss angles less than 10^{-6} with synthetic silica. This is why it has been proposed to use sapphire instead. Unfortunately sapphire has bad optical properties, so that it could not be used for transmitting mirrors.

3.3.3 Alternative Beam geometries

The third parameter on which to act is U, which leads to look for beam profiles that decrease that (virtual) mirror strain. In the current situation, the optical beams circulating in the interferometers are the gaussian beams emitted by standard lasers in which optical power is focused on a small spot at the center of the mirror. A way of calculating U has been found in [15] when total axisymmetry is assumed. A first approximation, valid if the hot spot radius is small compared to the mirror size, and a Gaussian TEM_{00} mode of parameter w, having thus an intensity profile of the form :

$$I(r) \;=\; \exp\left[-2r^2/w^2\right]$$

is simply, regarding the mirror substrate as an semi-infinite medium :

$$U \;=\; \frac{1-\sigma^2}{2\sqrt{\pi}Yw}$$

where Y is the Young modulus of the substrate and σ its Poisson ratio. This makes clear that it is desirable to increase parameter w. For larger values of w, the assumption of a semi-infinite medium cannot be kept, and the dimensions of the (cylindrical) substrate, its radius a and its thickness h must enter the model. For summarizing the result, U is the sum of two contributions :

$$U \;=\; U_0 + \Delta U$$

that can be computed separately. Some notation must be recalled. The $J_\nu(x)$ are the ordinary Bessel functions and $\{\zeta_k,\ k \in \mathbb{N}^*\}$ the discrete family of all non-zero solutions of $J_1(\zeta) = 0$. Let us note $x_k \equiv \zeta_k h/a$ and $q_k \equiv \exp(-2x_k)$. If now the intensity distribution in the readout beam is $I(r)$, we can define its Fourier-Bessel coefficients as:

$$p_k \;=\; \frac{2\pi}{J_0^2(\zeta_k)}\int_0^a I(r)J_0(\zeta_k r/a)\,r\,dr$$

and an auxiliary parameter ξ as

$$\xi = \sum_{k>0} \frac{p_k J_0(\zeta_k)}{\zeta_k^2} \tag{19}$$

Finally, U_0 can be expressed as the following series :

$$U_0 = \frac{1-\sigma^2}{\pi a Y} \sum_{k>0} \frac{J_0^2(\zeta_k) p_k^2}{\zeta_k} \frac{1-q_k^2+4q_k x_k}{(1-q_k)^2-4q_k x_k^2} \tag{20}$$

and ΔU, using 19 as :

$$\Delta U = \frac{a^2}{6\pi h^3 Y} \left[\left(\frac{h}{a}\right)^4 + 12\sigma\xi \left(\frac{h}{a}\right)^2 + 72(1-\sigma)\xi^2 \right] \tag{21}$$

At this point, all the thermal noise PSD amounts to compute the beam-profile coefficients p_k. For a TEM_{00} mode as above :

$$p_{k,0}^{(0)} = \frac{1}{J_0^2(\zeta_k)} \exp\left[-\frac{\zeta_k w^2}{8a^2}\right]$$

A way of obtaining a more homogeneously distributed light power by using special mirrors such that the cavity eigenmodes are "flat top" beams has been proposed [16]). If we adopt a simple model in which the intensity is assumed constant on a disk of radius $b < a$ and zero outside, the corresponding profile coefficients p_k are :

$$p_{k,flat} = \frac{2aJ_1(\zeta_k b/a)}{b\zeta_k J_0^2(\zeta_k)}$$

For instance, with a $b = 11.3$ cm, for a Virgo mirror ($a = 17.5$ cm, $h = 10$ cm) a gain factor of about 3 could be achieved in the LSD with respect to the present situation [17] . This kind of optical modes are however obtained in a Fabry-Perot cavity by using non spherical mirrors. Some numerical and experimental R&D studies have been carried out [18] to test the operation of such cavity from the point of view of optical stability under small misalignments.

Recently it has been proposed [19] to use high order TEM modes, to obtain a more homogeneous power distribution. These modes at the same time allow a better noise reduction and keep a spherical wavefront. The profile coefficients for a Laguerre-Gauss mode $\mathrm{LG}_{n,m}$ are :

$$p_{k,m}^{(n)} = \frac{1}{J_0^2(\zeta_k)} \exp\left[-\frac{\zeta_k w^2}{8a^2}\right] L_m\left(\frac{\zeta_k w^2}{8a^2}\right) L_{m+n}\left(\frac{\zeta_k w^2}{8a^2}\right)$$

where the $L_n(x)$ are the Laguerre polynomials. For instance a $\mathrm{LG}_5^{(5)}$ mode with $w = 3.5$ cm used as a readout beam for a mirror of diameter $2a = 35$ cm and thickness $h = 10$ cm (Virgo parameters) could achieve a gain of about 5 in sensitivity with respect to the present situation in Virgo, without significant increase in diffraction losses. An important point is that this allows to keep spherical mirrors.

3.4 Issues in Optical technology

3.4.1 Technology

The shot-noise limited sensitivity of $2\,10^{-23}\,\mathrm{Hz}^{-1/2}$ that has been shown above theoretically feasible rests on a good reflectance of the Michelson subsystem, i.e. a reflectance allowing to get the required surtension $\mathcal{S} \sim 50$ in the recycling cavity. It is easily seen that the maximum $\mathcal{S}$ is:

$$\mathcal{S}_{\max} = \frac{1-p_r}{1-(1-p_r)(1-p_s)^2(1-\sigma)^2}$$

where p_r, p_s are the losses at the recycling mirror and at the splitter respectively, whereas σ is the coupling rate of the cavities defined above (16). These losses are dominated by the coupling rate (by a factor comparable to the finesse), so that a rough estimate of the maximum gain is:

$$\sqrt{\mathcal{S}_{\max}} \;=\; \frac{1}{\sqrt{2\sigma}} \;=\; \frac{1}{\sqrt{4p\mathcal{F}/\pi}}$$

For having $\mathcal{S} \geq 50$ with $\mathcal{F} = 50$, the overall losses must therefore be less than 300 ppm. These losses involve not only thermalization of light, but also scattering (roughness of the reflecting surfaces), diffraction (aberration) and misalignments, so that this figure of 300 ppm is demanding. Scattering losses scale as $1/\lambda^2$. A special synthetic silica has been developed specially for Virgo & LIGO in order to make very low absorption substrates, a specific polishing protocole has been defined with a manufacturer for obtaining superpolished surfaces. Then the polished surface becomes reflecting after a coating process in which stacks of dielectric layers with alternative low and high refractive indices are deposited. The wavelength of $\lambda \sim 1.064\,\mu$m is the best found compromise allowing powerful light sources (Nd:YAG lasers) and low scattering losses (< 1 ppm). This coating process was first developed for very small highly reflecting mirrors involved for instance in laser gyros. Extension to large surfaces (~ 35 cm) was a challenge. A specific facility has been built at the IPN-Lyon, able to process large diameter samples in a clean environment [20].

3.4.2 Simulation

It was and still is difficult to assess the optical requirements without a numerical modelization of the interferometer. This is why a special code has been developed [21]. The main point is to represent light propagation from a given plane to a next one at a finite distance L. In the paraxial approximation of wave optics, if we call $A(x, y)$ the wave complex amplitude at abscissa $z = 0$, coordinates (x, y) being defined in the transverse plane and $B(x, y)$ the diffracted amplitude at $z = L$ is obtained from the Fresnel integral, provided the diffraction angles are not to wide (paraxial) :

$$B(x,y) \;=\; \int_{\mathbb{R}^2} K_L(x-x', y-y')\, A(x',y')\, dx'\, dy' \tag{22}$$

where the function $K_L(x, y)$ is the diffraction kernel (λ is the wavelength and $k \equiv 2\pi/\lambda$):

$$K_L(x,y) \;=\; -\,\frac{i}{\lambda L}\,\exp\left[ik\,\frac{x^2+y^2}{2L}\right]$$

(22) being a convolution product, it can be expressed under the form of a Fourier transform. If the Fourier coordinates conjugate from (x, y) are denoted by (p, q), we have :

$$\tilde{B}(p,q) \;=\; \tilde{K}_L(p,q) \times \tilde{A}(p,q)$$

The Fourier transform $\tilde{K}_L$ (propagator) has an explicit expression :

$$\tilde{K}_L(p,q) \;=\; \exp\left[-iL\,\frac{p^2+q^2}{2k}\right]$$

The point is that reduced to Fourier transforms, the propagation problem can be treated via Fast Fourier Transform algorithms which allows very efficient codes. The way of propagating a wave amplitude is thus

- take the 2D-FFT of $A(x, y)$
- multiply by the propagator (it has been computed once for all)

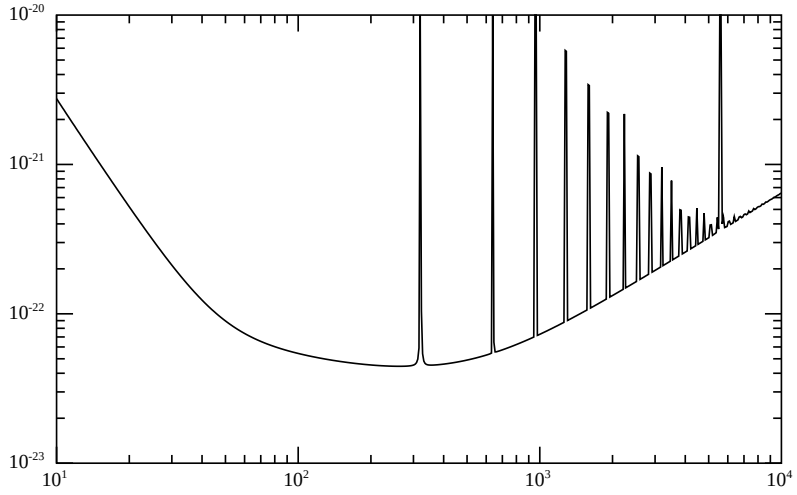

Figure 5: Nominal (theoretical) spectral sensitivity of Virgo

- take the reciprocal 2D-FFT and get $B(x, y)$.

This method is especially efficient in the case of resonant cavities. For instance, consider the equation (12) for intracavity amplitude $A_{\rm ic}(x, y)$ inside a cavity from an incoming amplitude $A_{\rm in}(x, y)$. It can be generalized as :

$$A_{\rm ic} \;=\; M_{1,\rm trans} A_{\rm in} + M_{1,\rm ref}.\mathcal{P}.M_{2,\rm ref}.\mathcal{P}.A_{\rm ic} \tag{23}$$

where the linear operator P refers to the sequence detailed above and the $M_{\rm i,ref,trans}$ to phase plates equivalent to the mirrors properties (geometry of the surface, transmission chart). An explicit algebraic solution formally exist but provides no realistic computation scheme. A realistic method is to take an initial guess for $A_{\rm ic}$ (for instance the theoretical mode assuming perfect mirrors) and iterating (23) until a given accuracy is met. This is the basic principle of DarkF, a code developed within the Virgo collaboration after [21]. This method allows to treat imperfect beams and imperfect mirrors. It is possible to import in the code measured maps for all mirrors and give tilt angles, detunings in order to check the performances of the resulting virtual interferometer versus the nominal estimations.

3.5 Planned spectral sensitivity

Owing to the preceding discussion, the overall spectral sensitivity is an envelope, resulting at low frequency (< 50 hz) from the pendulum thermal noise, in the intermediate range around 100 Hz from the mirrors internal thermal noise, and in the upper part of the spectrum from shot noise. At the resonances of the suspension wires, thin peaks appear. The foreseen sensitivity curve, after reduction of non-essential noises has the shape summarized on Fig.5.

3.6 Frequency Stabilization

Frequency fluctuations of the source laser result in a specific noise on the detection channel. If the random process $\delta\nu(t)$ denotes these frequency fluctuations, the corre-

sponding phase fluctuations on the dark fringe are

$$\delta\Phi(t) \;=\; \frac{d}{L}\,\frac{2\pi L}{c}\,\delta\nu(t) \tag{24}$$

where L is the mean length of the arms and d their difference. For a simple short Michelson interferometer, it is easy to carefully tune the arm lengths to obtain an arbitrarily low level of noise. For a long baseline interferometer with resonant cavities, the effective length $L_{\rm eff} = (2\mathcal{F}/\pi)\times L$ depends not only on the geometrical length L of the arms, but also on the finesses of the cavities. These finesses depend in turn on the reflection coefficients of the mirrors, so that the noise level is eventually determined by the ability of technology to produce mirrors with very close reflectivities, allowing to make as symmetrical cavities as possible. We have seen that the phase shot noise LSD is

$$S_\Phi^{1/2}(f) \;=\; \sqrt{\frac{2\hbar\omega}{\mathcal{S}P_L}}$$

We can rewrite (24) in terms of LSD, by asking the frequency fluctuations to produce a phase noise lower than the shot noise:

$$\frac{S_{\delta\nu}^{1/2}}{\nu_L} \;<\; \frac{\lambda}{4\mathcal{F}L}\,\frac{\mathcal{F}}{\Delta\mathcal{F}}\sqrt{\frac{2\hbar\omega}{\mathcal{S}P_L}}$$

where $\Delta\mathcal{F}$ represents the difference between the finesses of the North and West cavities. With the same values as above, assuming $\mathcal{S}P_L$ ∼1 kW reaching the splitter, a mean cavity finesse of $\mathcal{S}\sim 50$, this is:

$$S_{\delta\nu}^{1/2} < \frac{10^{-8}}{\Delta\mathcal{F}/\mathcal{F}}\ \text{Hz.Hz}^{-1/2}$$

with a symmetry rate of 1% for the finesse, we obtain a requirement of

$$S_{\delta\nu}^{1/2} < 10^{-6}\ \text{Hz.Hz}^{-1/2}$$

This very strong requirement is satisfied by at least two stages of frequency control. A first stage is a servo loop using error signals by comparison of the laser frequency with a reference passive, very stable resonant cavity (long term stabilization). A second stage is a servo loop on the common mode of the two long arms (short term stabilization). The result is one the most stable oscillators in the present metrology status. Obtaining at the same time an output power of about 20W is obtained via the injection technique, in which the stabilized laser light enters a powerful slave laser whose mode is locked on the master wave.

3.7 Data Analysis

The order of magnitude of the sensitivity makes likely a very poor signal to noise ratio at least in the present generation of antennas. This is why special signal processing techniques have been developed for extracting GW signature from the dominant instrumental noise background (or foreground ?). Expected signals are:

- short bursts (a few ms) possibly produced by supernova or exotic cosmic string events
- permanent waves emitted by fast pulsars having some quadrupolar moment
- chirps emitted during the inspiral/merging/ringdown process of binary coalescence

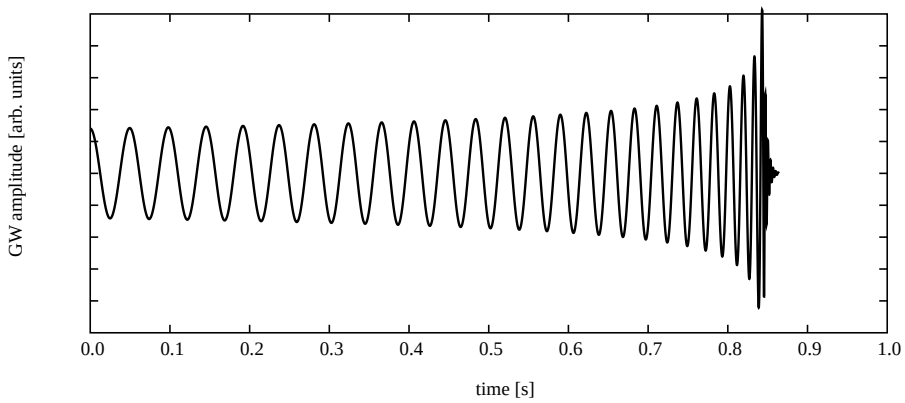

Figure 6: Coalescence signal for two black holes of equal mass (30 solar masses)

For the detection of binary black hole (BBH) coalescence, the common strategy of all groups is to use the matched filtering technique. It is possible to accurately describe the inspiral phase either by using the Parametrized Post Newtonian approach [5] or the Effective One Body method [22], or by numerical simulations. The result provides families of templates (each corresponding to a point in the parameter space). An example can be seen on Fig.6 for a two 30 solar masses BBH. The signal is assumed to enter the detection band at the date at which its frequency is 20 Hz. The total duration is less than 2s. Detection amounts to look for a correlation peak between the interferometer output and a bank of templates.

3.8 Present status

The two american LIGO instruments at Hanford (WA) and Livingston (LA) are already operating at their nominal sensitivity. The size of the LIGO antennas is 4 km. At the Hanford site, one more antenna is installed in the same vacuum pipe, with 2 km size. The French-Italian Virgo at Cascina (Italy) of size 3 km comes at the end of its commissioning phase. The Virgo sensitivity is already comparable to the american antennas at high frequency (see Fig.7). A German-British antenna GEO600 of size 600 m is operating since 2002 near Hannover. Its sensitivity remains less than larger antennas (see Fig.8), but alternative optical designs could allow to reach a comparable sensitivity at the price of a reduced bandwidth. A Japanese antenna of size 300 m, TAMA [24] is operating since 2003, the best sensitivity being about $10^{-}21\mathrm{Hz}^{-1/2}$ (see Fig.9).

4 The LISA mission

LISA is the present status of a very old idea initiated in the seventies and aiming to receive and analyze very low frequency GW from sources involving massive black holes. There is on Earth a “wall” at a few Hz that forbids, due to direct direct Newtonian attraction of test mirrors by ground motions, going to lower frequencies. The solution is therefore in space. LISA is an ambitious ESA/NASA joint mission which consists in three spacecraft forming a triangle of 5 Mkm a side, in orbit around the Sun 50 Mkm behind the Earth. The three spacecraft are optically linked by six Nd:YAG laser beams. The GW signature is read on the six Doppler data flows (beat note of the incoming light against the local oscillator). LISA is expected to fly in

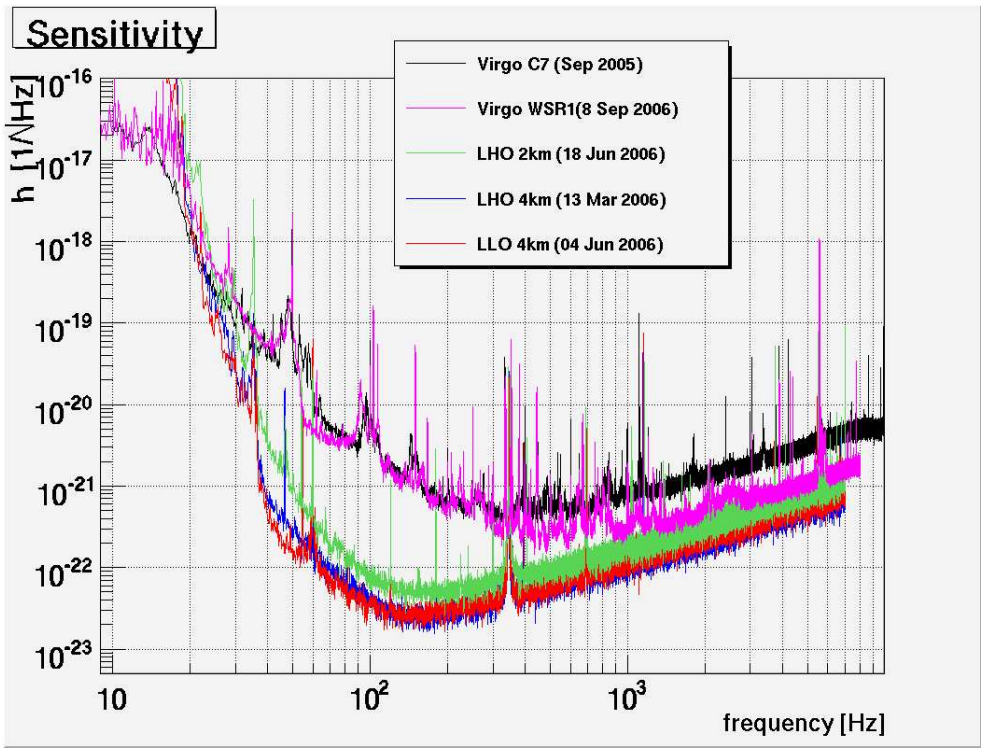

Figure 7: Compared sensitivities of LIGO and Virgo antennas (LLO=LIGO Livingstone Observatory, LHO=LIGO Hanford Observatory, WSR=Weekly Science Run, C=Commissioning)

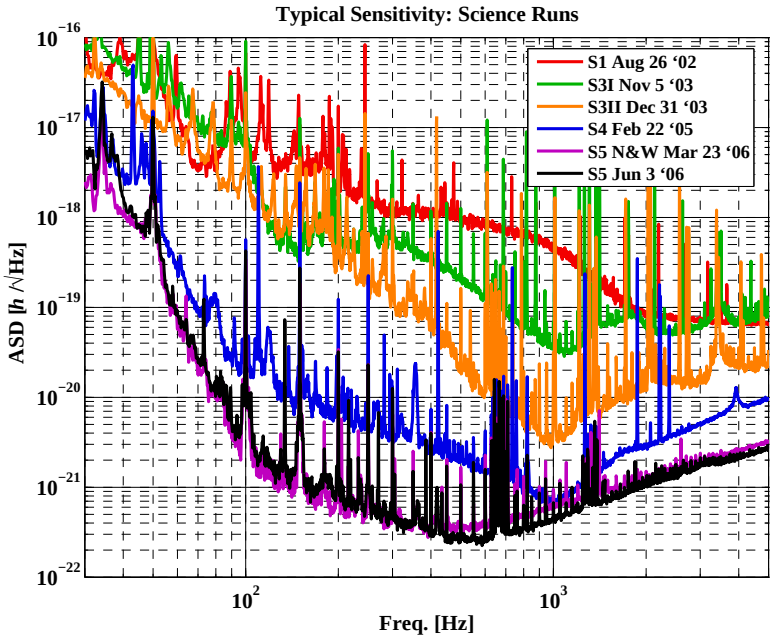

Figure 8: GEO600 typical sensitivity (after[23])

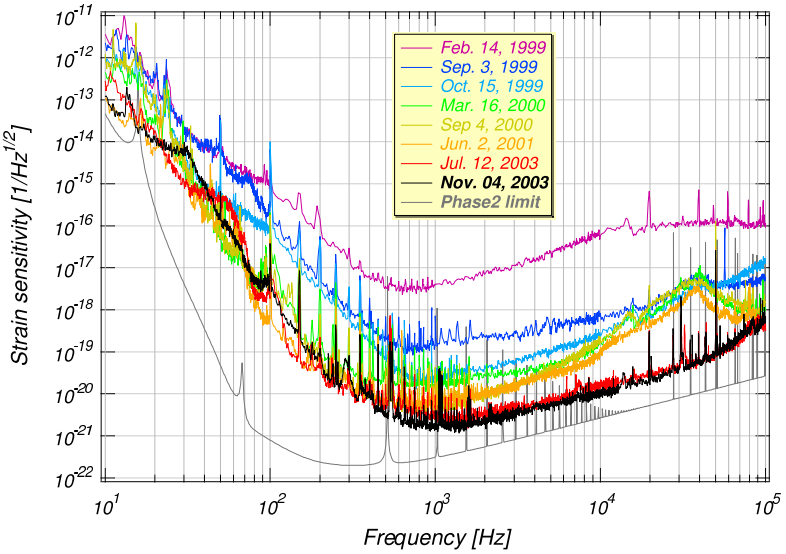

Figure 9: TAMA300 typical sensitivity (after[24])

2014 if the project passes a review in 2008 against a few others fundamental physics missions, and if the technological demonstrator LISA-Pathfinder is successful.

4.1 Orbital configuration

The stability of a large triangular formation on heliocentric orbits is not trivial. It can be shown (e.g. [25]) that it is possible by combining slightly elliptical, slightly inclined orbits. More specifically, let L be the inter-spacecraft distance ($L \sim 5\,10^9$m) and R the radius ($R \sim 1.5\,10^{11}$m) of the almost circular terrestrial orbit. Let us define the small parameter $\alpha = L/2R \sim 1/60$. We can chose simultaneously for the orbit of spacecraft #1 an inclination angle of ϵ with respect to ecliptic, and an eccentricity of e. The right choice is :

$$\epsilon \;=\; \arctan\left[\frac{\alpha}{1+\alpha/\sqrt{3}}\right] \quad \text{and} \quad e \;=\; \sqrt{1+\frac{2\alpha}{\sqrt{3}}+\frac{4\alpha^2}{3}}-1$$

In barycentric coordinates (centered on the Sun with (x, y) axes in the ecliptic and fixed with respect to far stars), the motion of spacecraft #1 has the parametric form:

$$\left\{\begin{array}{rcl} x &=& R(\cos E_1 - e)\cos\epsilon \\ y &=& R\sqrt{1-e^2}\,\sin E_1 \\ z &=& -\,R(\cos E_1 - e)\sin\epsilon \end{array}\right. \tag{25}$$

where $E_1(t)$ is the so-called eccentric anomaly implicitly defined by

$$E_1 - e\,\sin E_1 \;=\; \Omega t$$

where $\Omega \equiv 2\pi/(1\text{ year})$. The orbits of spacecraft #2 and 3 are obtained by

- Shifting by 120 degrees the eccentric anomaly, so that

$$E_i - e\,\sin E_i \;=\; \Omega t - (i-1)\frac{2\pi}{3} \quad (i = 1, 2, 3)$$

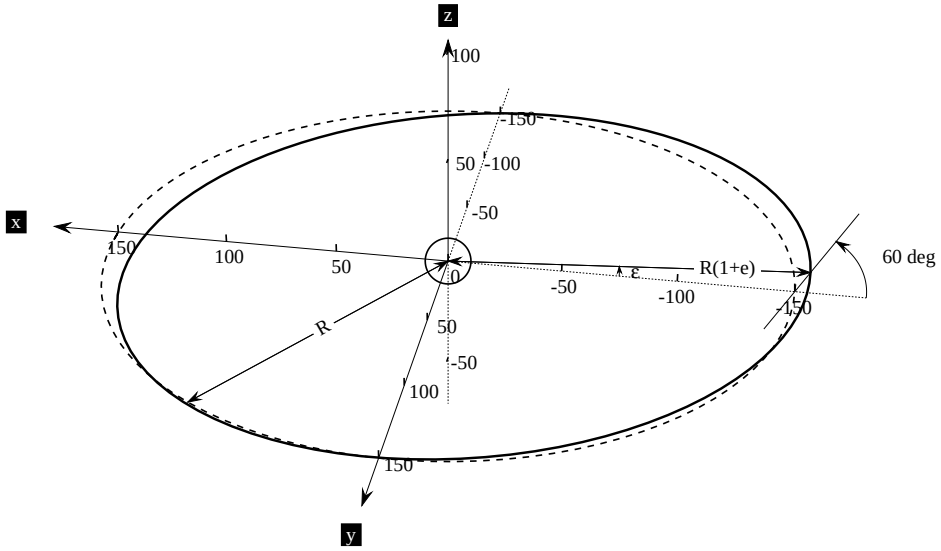

Figure 10: Solid: Orbit of spacecraft #1. Dashed: Earth's orbit (ecliptic)

- Rotating the semi-major axes by 120 degrees in the (x, y) plane, so that the motions of all spacecraft are parametrized by::

$$\left\{ \begin{array}{lcl} X_i &=& x_i \cos\theta_i \; - \; y_i \sin\theta_i \\ Y_i &=& x_i \sin\theta_i \; + \; y_i \cos\theta_i \\ Z_i &=& z_i \end{array} \right. \tag{26}$$

  where $\theta_i \equiv (i-1) \times 2\pi/3$, and where the (x_i, y_i, z_i), $i = 1, 2, 3$ are parametrized according (25) with the E_i.

The result is that the three spacecraft are located in a plane making an angle of 60 degrees with respect to ecliptic, with mutual distances constant at first order in α, making a triangle rotating around its mass center with a 1 year period (see Fig.10). "At first order in α" means that a more accurate evaluation shows a deformation of the triangle, and inter-spacecraft distances variable by about 100,000 km. It is possible to reduce this "flexing" to less than 50,000 km by slightly increasing the 60 degrees angle [26].

4.2 Drag free operation

At the level of $\Delta L/L \sim 10^{-22}$, meaning a $\Delta L \sim 5\,10^{-12}$m, it is clear that perturbations caused by solar winds must be strongly rejected. It is therefore planned to operate LISA under the drag free regime. This means that the spacecraft protecting shell is served on an internal reference mass by a capacitor readout system. The free falling reference mass plus the readout system form an accelerometer. This kind of accelerometer has been imagined and successfully flied by the french ONERA on several space missions [27], but here the targetted readout noise is about $3\,10^{-15}\,\mathrm{m.s^{-2}Hz^{-1/2}}$ in a frequency range from 10^{-4} Hz to 10^{-1} Hz. The model relevant for LISA has been developed following analogous principles. Controlling the spacecraft position with respect to the test mass requires controlled forces. These forces are applied by micro-thrusters. Two systems are being proposed and will be tested in the "LISA PAthfinder" demonstration mission.

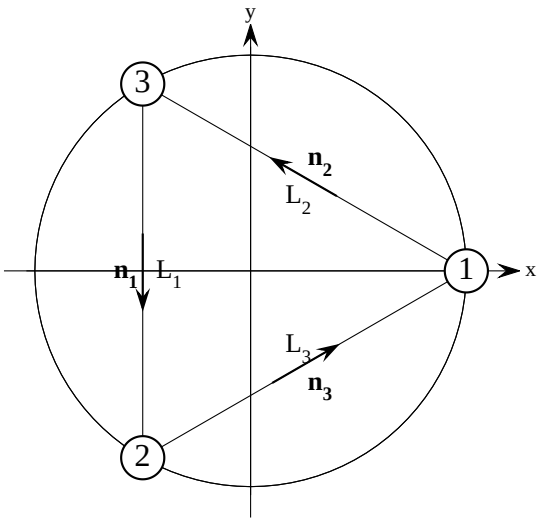

Figure 11: Notations for the LISA geometry

4.3 Data flow

In a very simplified scheme, the LISA readout system involves six phasemeters, each delivering its own data flow. If we call $C_i(t)$ $(i = 1, 2, 3)$ the instantaneous frequencies aboard the three spacecraft , the apparent Doppler measurement on board spacecraft #1 for light coming from spacecraft #2 is (counterclockwise) according to (10):

$$V_1 \;=\; \left[\frac{\delta\nu(t)}{\nu}\right]_{2\to 1} \;=\; \frac{H(t-\mathbf{w}.\mathbf{x}_1) - H(t-\mathbf{w}.\mathbf{x}_2 - L_3)}{2(1-\mathbf{w}.\mathbf{n_3})} + \tag{27}$$

$$+\, C_1(t) - C_2(t-L_3) + s_1(t)$$

(see Fig.11) $s_1(t)$ accounts for the shot noise generated by the detection process on board spacecraft #1. We take into account the fact that the triangle may be not equilateral, so that we have to deal with three different lengths L_i $i = 1, 2, 3$. The data flows V_2, V_3 can be obtained by cyclic permutation of the indices. For the clockwise links, we get

$$U_2 \;=\; \left[\frac{\delta\nu(t)}{\nu}\right]_{1\to 2} \;=\; \frac{H(t-\mathbf{w}.\mathbf{x}_2 - L_3) - H(t-\mathbf{w}.\mathbf{x}_1)}{2(1+\mathbf{w}.\mathbf{n_3})} + \tag{28}$$

$$+\, C_1(t-L_3) - C_2(t) + s_2(t)$$

The data flows U_3, U_1 are obtained by cyclic permutation of indices.

It seems that the signal ($\sim 10^{-22}$), due to the huge asymmetry between the optical path of the long link (5 Mkm) and the local path (~ 1 m) is largely dominated by the frequency noises of the lasers (the C_i, $\sim 10^{-13}$ Hz$^{-1/2}$ under closed stabilization loop). Fortunately, the number of data flows allows some redundancy leading to a dramatic reduction of the noise.

4.4 Time Delay Interferometry

We can define three delay operators D_i via their action on any function of time f:

$$(D_i f)(t) \;=\; f(t - L_i)$$

If we consider the part of the Doppler data due to laser noise, we can write:

$$\begin{array}{rcl} U_1 &=& D_2C_3 - C_1 \\ U_2 &=& D_3C_1 - C_2 \\ U_3 &=& D_1C_2 - C_3 \\ V_1 &=& C_1 - D_3C_2 \\ V_2 &=& C_2 - D_1C_3 \\ V_3 &=& C_3 - D_2C_1 \end{array} \tag{29}$$

It has been remarked that some combinations of the U_i, V_i give an identically zero result, and can be regarded as noise canceling. Use of such noise canceling combinations was proposed by M. Tinto [28] and called "Time Delay Interferometry" (TDI). The algebraic structure of TDI has been found and explained in [11]. The simplest example is found by considering the C_i U_i and the V_i as vectors $\mathbf{C}$, $\mathbf{U}$, $\mathbf{V}$ and the delay operators D_i as the components of a vector operator $\mathbf{D}$. The sum $\mathbf{U}+\mathbf{V}$ has the algebraic signature of a curl:

$$\mathbf{U}+\mathbf{V} \;=\; \mathbf{D}\times\mathbf{C}$$

It is now clear that the "divergence" of $\mathbf{U}+\mathbf{V}$ is identically zero, so that

$$\mathbf{D}.(\mathbf{U}+\mathbf{V}) \;=0 \;\;\Rightarrow\;\; \sum_{i=1}^{3} D_iU_i + \sum_{i=1}^{3} D_iV_i \;=\; 0$$

Each noise canceling ("silent") combination y can thus be represented by a 6-uple $Y = (p_i, q_i)$ of polynomials in the formal variables D_i, acting on the data 6-uple $U = (V_i, U_i)$:

$$y \;=\; \langle Y|U\rangle \;=\; \sum_{i=1}^{3}(p_iV_i + q_iU_i)$$

The basis of TDI is the set $\mathcal{S}$ of all silent Ys. It has been shown [11] that $\mathcal{S}$ has the algebraic structure of a first module of syzygies on the ring of formal polynomials. This means that any element of $\mathcal{S}$ can be obtained by a linear combination whose coefficients are polynomials in D_i, of generators of $\mathcal{S}$. A generating part of $\mathcal{S}$ has been found by [28], containing :

$$\zeta \;=\; (\mathbf{p},\mathbf{q}) \;=\; (D_1, D_2, D_3, D_1, D_2, D_3)$$

with the new silent 6-uple :

$$\alpha \;=\; (1,\; D_3,\; D_1D_3,\; 1,\; D_1D_2,\; D_2)$$

plus its two successive circular permutations (of indices and of locations in the sub-3-uples):

$$\begin{array}{rcl} \beta &=& (D_1D_2,\; 1,\; D_1,\; D_3,\; 1,\; D_2D_3) \\ \gamma &=& (D_2,\; D_2D_3,\; 1,\; D_1D_3,\; D_1,\; 1) \end{array}$$

Any combination of α, β, γ applied to the data 6-uple $\mathbf{U}$ is thus laser noise free. It can be shown that the same combination is still sensitive to GW. Generator ζ (often called "symmetric Sagnac") strongly attenuates the GW signals at low frequency. There is no hope however to suppress the shot noise nor the noise coming from the accelerometer readout system, because those are purely local noises (not transmitted to other spacecraft with some delay). The global sensitivity curve for a typical TDI combination ("Michelson") is shown on Fig.12. It assumes one year integration time for a permanent source, with a signal to residual noise ratio of 5, and an average on the angular coordinates of the source. In reality, the situation is more complex because there are six lasers, not three, and the propagation times between two spacecraft are not reciprocal, due for instance to the Sagnac effect in rotating frames, and are even variable in time due to the flexing effect. But the preceding method remains valid in principle, up to improvements [29],[30].

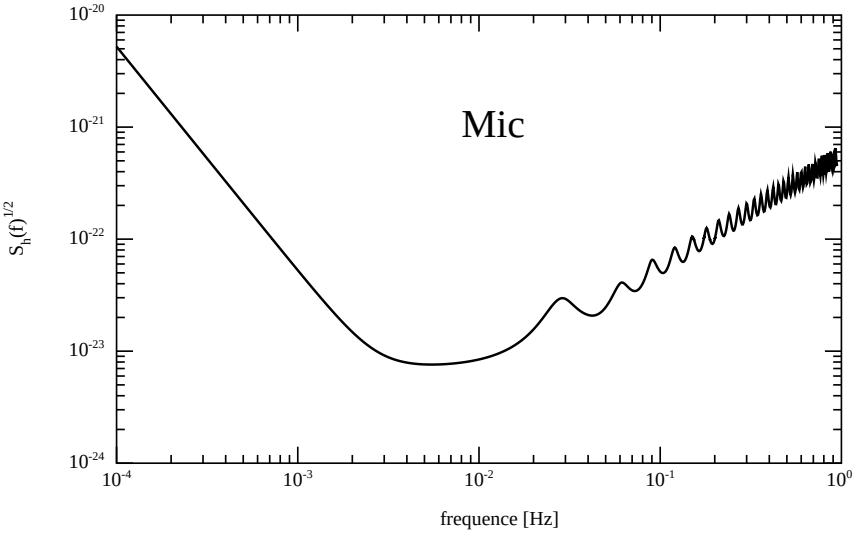

Figure 12: Mean spectral sensitivity of LISA for the "Michelson" TDI combination

4.5 Data analysis

Owing to the low frequency domain of sensitivity, the sampling frequency may be taken at a fraction of a Hz, so that the flow of data down to Earth is consistent with the bandwidth of the microwave link. A preprocessing by TDI generators is necessary, which implies a good knowledge of the instantaneous inter-spacecraft distances. Depending on the kind of source to be studied, several strategies may be developed.

A major point is the existence of a foreground of GW noise generated by the population of galactic compact binaries (involving neutron stars, white dwarfs, black holes) whose orbital frequencies (times 2) fall within the detection band of LISA. The GW amplitude resulting from all these monochromatic sources is analogous to a stochastic background. These objects are a huge number (e.g. $\sim 10^8$ white dwarf binaries, see [31]), All of these produce a so-called confusion noise the spectral density of which is dominant at very low frequency (from 0.1 to 1 mHz). For detecting a particular binary, it is possible to find optimal combinations of the generators [32] and even combinations giving a zero result, allowing to selectively suppress known sources [33],[32] for a "coronographic" operation of LISA.

The signals generated by or around black holes are of two types.

- Stellar class objects orbiting supermassive black holes have complex inspiralling trajectories ending by a capture. The models for such events are called Extreme Mass Ratio Inspirals (EMRI). The GW emitted during EMRI have a complex frequency structure [34]. These models depend on a number of parameters making difficult a matched filtering approach. Moreover, situations may happen in which several bodies are involved resulting in a perturbed process escaping the "simple" model. Time-Frequency methods based on wavelet transforms seem a relevant tool.

- Supermassive Binary Black Holes (SMBBH) are expected to inspiral on a long time period. The final phase could be observed during several years of LISA operation. A matched filtering approach is possible, and Time-Frequency methods as well.

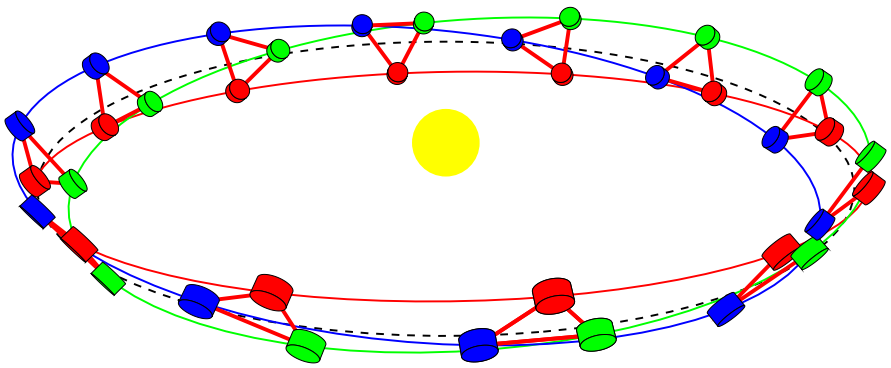

Figure 13: Orbital evolution of LISA after "LISACode"

4.6 Simulators

The closest date of launch of the mission being 2014, the various algorithms building the Data Analysis System must be developed and tested with synthetic data. Two data simulators have been coded in the United States and one in France:

- Synthetic LISA at the Jet Propulsion Laboratory (Pasadena, California) [35]
- The LISA Simulator at Montana U. [36]
- LISACode by LISA-France (APC, Observatoire de la Côte d'Azur) [37] (see Fig.13)

The simulators compute the orbital motion (26) of each spacecraft and the corresponding transfer function (27,28) for the GW signals. The GW amplitudes for several kind of sources and angular locations are read from files and the result is given in terms of TDI generators.

5 Conclusion

The first generation of ground GW antennas is now beginning to deliver science data. Technological improvements will probably be needed to achieve a better sensitivity which could improve the rate of detected events. Ideas already exist for improving the laser power and for reducing the thermal noise, which were the main obstacles to overcome. The fate of the large space antenna LISA will depend on the willing of the Relativistic Astrophysics community to continue the international cooperation that began so long ago.

References

[1] `http://www.ligo.caltech.edu`

[2] `http://wwwcascina.virgo.infn.it`

[3] `http://lisa.jpl.gov`

[4] Kip S. Thorne, in 300 years of gravitation, Edited by S.W.Hawking and W. Israel, Cambridge U.P. 1987.

[5] L. Blanchet, Phys. Rev. D **72**, 044024 (2005).

[6] Joseph Weber, in Gravitation and Relativity, Edited by Chiu and Hoffmann, Benjamin 1964.

[7] J.-Y. Vinet, Ann. Inst. Henri Poincaré, Vol. XXX n3 (1979) p. 251.

[8] L. Baggio et al., Phys. Lett. **95** (2005) p. 081103.

[9] P. Astone et al., Class. Quant. Grav. **23** (2006), S57-S62.

[10] A. de Waard et al., Proceedings of the 6th Amaldi Conference on Gravitational Wave, Okinawa, Japan (2005), (to be published in Jour. of Phys. : Conference series).

[11] S.V. Dhurandhar, R.K. Nayak and J-Y. Vinet, Phys. Rev. D **65** (2002), 102002.

[12] Ronald Drever, in *Gravitational Radiation*, edited by N. Deruelle and T. Piran (North Holland 1983) p. 321.

[13] T. Uchiyama et al., Class. Quantum Grav. **21** (2004), S1161–S1172.

[14] Yu. Levin, Phys. Rev. D **57** (1998), p. 659.

[15] F. Bondu, P. Hello and J.-Y. Vinet, Phys. Lett. A **246** (1998), p. 227–236.

[16] E. D'Ambrosio, Phys. Rev. D **67** (2003), 102004.

[17] J.-Y. Vinet, Class. Quantum Grav. **22** (2005), p. 1395.

[18] J. Agresti et al., LIGO technical documents, `http://www.ligo.caltech.edu`

[19] B. Mours, E. Tournefier, J.-Y. Vinet, Class. and Quantum Grav. **23** (2006), p. 5777–5784.

[20] `http://lma.in2p3.fr`

[21] P. Hello, N. Man, A. Brillet, J.-Y. Vinet, Journal de Physique I vol **2** (1992), p. 1287–1303.

[22] A. Buonanno, T. Damour, Phys. Rev. D **59** (1999), 084006.

[23] `http://www.geo600.uni-hannover.de`

[24] `http://tamago.mtk.nao.ac.jp`

[25] S. Dhurandhar, R. Nayak, S. Koshti, J.-Y. Vinet, Class. Quantum Grav. **22**, 3 (2005), p. 481–487.

[26] R. Nayak, S. Koshti, S. Dhurandhar, J.-Y. Vinet, Class. Quantum Grav. **26** (2006), p. 1763–1778.

[27] P. Touboul, A. Bernard, C.R. Acad. Sci. Paris Sér. IV (2001) p. 1271.

[28] M. Tinto, J. Armstrong, F. Estabrook, The Astroph. Journal **527** (1999), p. 814–826.

[29] M. Tinto, F. B. Estabrook, J. W. Armstrong, Phys. Rev D **69** (2004), 082001.

[30] R. Nayak, J.-Y. Vinet, Phys. Rev. D **70** (2004), p. 102003.

[31] G. Nelemans, L. Yungelson, S. Portegies Zwart, A&A **375** (2001), 890–898.

[32] R. Nayak, S. Dhurandhar, A. Pai, J.-Y. Vinet, Phys. Rev. D **68** (2003), 122001.

[33] M. Tinto, S. Larson, Class. Quantum Grav. **22** 10 (2005), S531–S535.

[34] S. Hughes, Class. Quantum Grav. **18** (2001), p. 4067–4073.

[35] http://www.vallis.org/syntheticlisa/

[36] http://www.physics.montana.edu/lisa/

[37] http://www.apc.univ-paris7.fr/SPIP/article.php3?id_article=164